Undergraduate Project Report

Student: Vishakha Goyal (221199)

Supervisor: Prof. Ushasi Roy

November 26, 2025

1 Introduction

This report documents the work done under UGP this semester. Dividing the work broadly, it includes, Simulations in ABAQUS and Literature Reviews. The research papers provided a detailed overview of hyperelasticity and different models used to evaluate hyperelastic materials under large strain, time dependence, high strain rate and hydrostatic condition. While doing the simulations, some unexpected results were obtained which sparked the curiosity of their origin and potential reason of the simulation results to differ from the previous findings of research paper. This does leads one to figure out if the findings proposed in different research papers is reliable or not, and what scenarios is it and is it not.

2 Simulations & Results

2.1 Simulating Mooney Rivlin Model under Uniaxial Tensile Testing

Test data (having stress-strain values): Abaqus documentation

Uniaxial Test Data (fed in ABAQUS)

Stress (MPa)	Strain
0.054	0.0380
0.152	0.1338
0.254	0.2210
0.362	0.3450
0.459	0.4600
0.583	0.6242
0.656	0.8510
0.730	1.4268

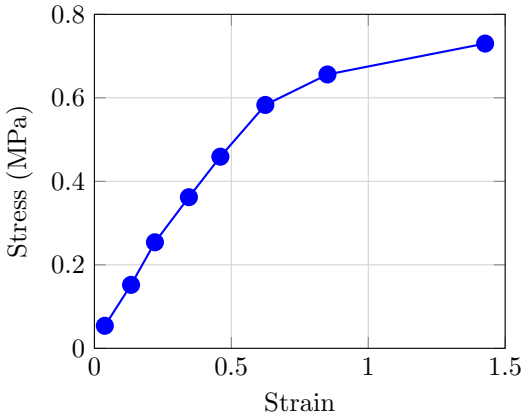

In Abaqus, a simulation was performed using the above material data with the Mooney–Rivlin hyperelastic model (isotropic) on a 30×30 mm 2D planar deformable block, with a displacement of 30 mm on one end while the opposite end was fixed (Figure 1).

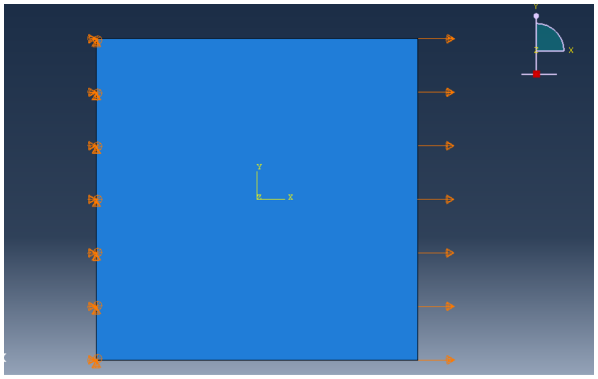

Figure 1: Model geometry and boundary conditions applied in Abaqus.

The results obtained were completely off from the trajectory of the original test data predictions. Therefore, several parameter sets were examined to determine whether the simulation results could be matched with the test data. Four different mesh configurations were evaluated using combinations of quadrilateral and triangular elements, with both linear and quadratic geometric order. However, the stress–strain response remained unchanged and showed no noticeable variation, even when altering mesh type, mesh density, or the element family (plane stress vs. plane strain).

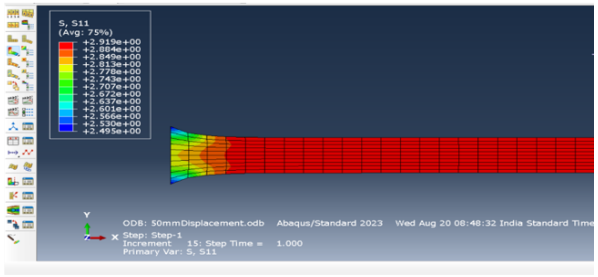

Figure 2: Tensile stress distribution along the specimen

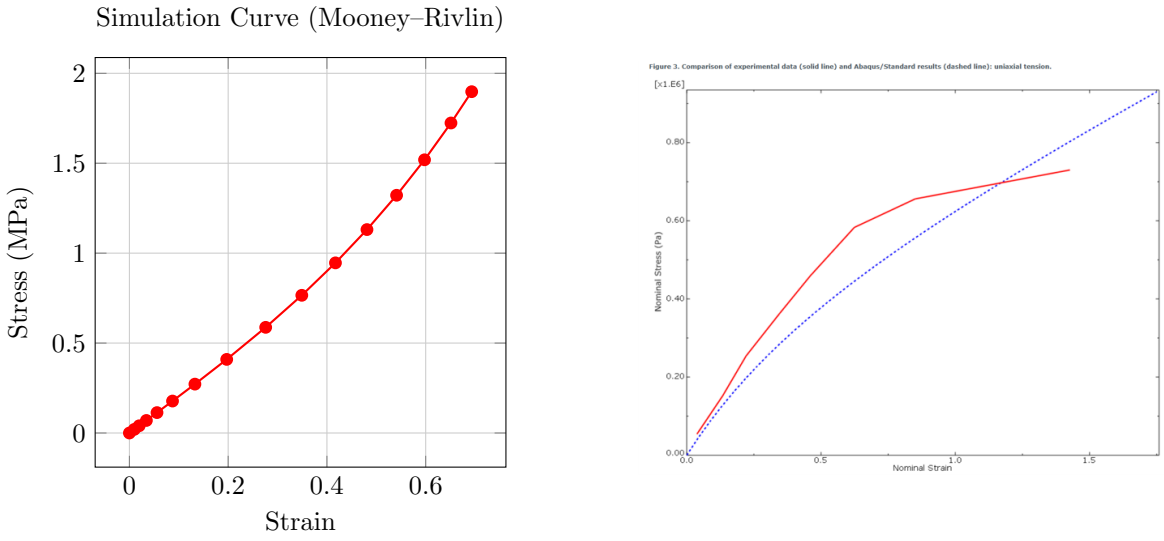

Figure 3: Comparison between ABAQUS Mooney–Rivlin simulation results (left) and experimental uniaxial test data (right).

Test Data (having values of coefficients): IJARIIE (Vol. 2, Issue 4, 2016)

. The paper provides material coefficients for hyperelastic models with different numbers of parameters (two-term, three-term, five-term and nine-term).

Table 1: Coefficients of Two-Parameter Mooney–Rivlin Material Model

C_{10} (MPa)	C_{01} (MPa)	D_1	Residual
0.287606	-0.25942	0	1.968622

Table 2: Coefficients of Nine-Parameter Mooney–Rivlin Material Model

C_{10}	C_{01}	C_{20}	C_{02}	C_{30}	C_{03}	C_{11}	C_{12}	C_{21}	D_1
2.996089	-3.0466	-135.056	-152.12	-10.018	-18.8031	283.4141	33.14071	0.128574	0

These coefficients were tested in Abaqus by fitting them to the corresponding hyperelastic models and evaluating material. However, it was found that the 2 parameter, Mooney Rivlin results (Figure 4) were again different and none of the other parameter sets resulted in a stable response during material evaluation under uniaxial loading, indicating that the direct use of the reported coefficients does not guarantee numerical stability.

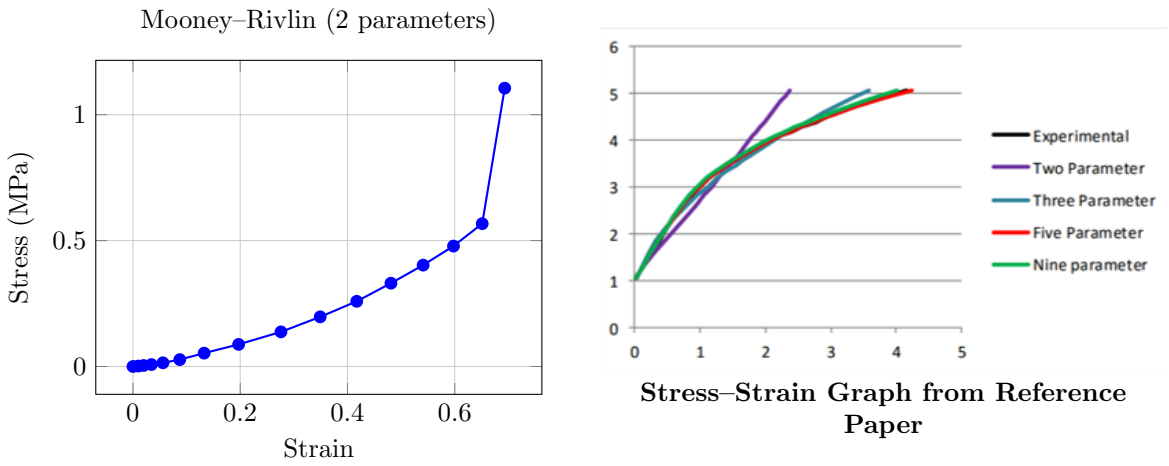

Figure 4: Comparison of Mooney–Rivlin 2-parameter simulation curve (left) with the stress–strain graph reported in the reference paper (right).

Alternate Test Data (having values of stress-strain)[1]

.

Table 2. Test results of stress-strain.

Force (F) N	Extension (ΔL) mm	Stress (σ) MPa	Strain (ε) %	Force (F) N	Extension (ΔL) mm	Stress (σ) MPa	Strain (ε) %
5	3.442	0.2924	0.0492	95	98.808	5.5556	1.4115
10	8.425	0.5848	0.1204	100	102.797	5.8480	1.4685
15	14.928	0.8772	0.2133	105	106.394	6.1404	1.5199
20	22.167	1.1696	0.3167	110	109.96	6.4327	1.5709
25	29.508	1.4620	0.4215	115	113.433	6.7251	1.6205
30	36.653	1.7544	0.5236	120	116.856	7.0175	1.6694
35	42.651	2.0468	0.6093	125	120.083	7.3099	1.7155
40	49.0000	2.3392	0.7000	130	123.469	7.6023	1.7638
45	54.512	2.6316	0.7787	135	126.999	7.8947	1.8143
50	59.899	2.9240	0.8557	140	130.365	8.1871	1.8624
55	65.118	3.2164	0.9303	145	133.637	8.4795	1.9091
60	69.943	3.5088	0.9992	150	136.928	8.7719	1.9561
65	74.579	3.8012	1.0654	155	140.153	9.0643	2.0022
70	78.972	4.0936	1.1282	160	143.472	9.3567	2.0496
75	83.394	4.3860	1.1913	165	146.861	9.6491	2.0980
80	87.387	4.6784	1.2484	170	150.262	9.9415	2.1466
85	91.232	4.9708	1.3033	175	153.557	10.2339	2.1937
90	95.236	5.2632	1.3605	178	156.181	10.4094	2.2312

(a) Experimental stress–strain data (tabulated).

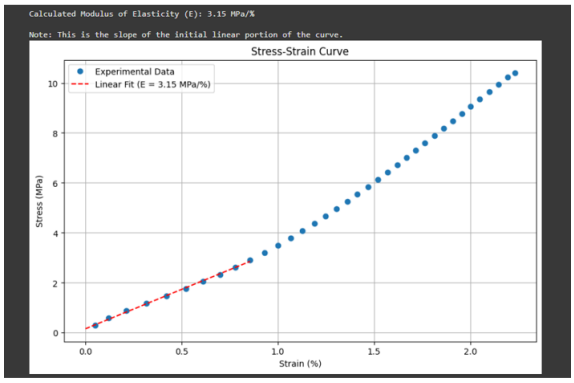

(b) Experimental stress–strain curve with linear fit.

Figure 5: Tensile test data from[1]

The test data was found to give numerically stable responses when fitted using a Polynomial hyperelastic model with $N = 2$ and an Ogden model with $N = 3$.
All simulations were performed on a 30 mm $\times$ 10 mm block in plane stress using a triangular mesh, with a prescribed displacement of 30 mm applied at one end.

Polynomial model ($N = 2$) – Simulation data

Strain	Stress (MPa)
0.00000	0.00000
0.00100	0.00678
0.00200	0.01353
0.00349	0.02360
0.00573	0.03857
0.00908	0.06077
0.01409	0.09347
0.02155	0.14125
0.03263	0.21028
0.04940	0.30851
0.07315	0.44587
0.10825	0.63509
0.15871	0.89624
0.22992	1.27390
0.32804	1.88859
0.45923	3.06346
0.62855	5.62607
0.69315	7.06411

(a) Polynomial hyperelastic model ($N = 2$).

Ogden model ($N = 3$) – Simulation data

Strain	Stress (MPa)
0.00000	0.00000
0.00100	0.00685
0.00200	0.01367
0.00349	0.02383
0.00573	0.03894
0.00908	0.06131
0.01409	0.09423
0.02155	0.14225
0.03263	0.21143
0.04940	0.30958
0.07315	0.44635
0.10825	0.63424
0.15871	0.89360
0.22992	1.27038
0.32804	1.88758
0.45923	3.06823
0.62855	5.63170
0.69315	7.06652

(b) Ogden hyperelastic model ($N = 3$).

Figure 6: Side-by-side comparison of simulation stress–strain datasets for Polynomial ($N = 2$) and Ogden ($N = 3$).

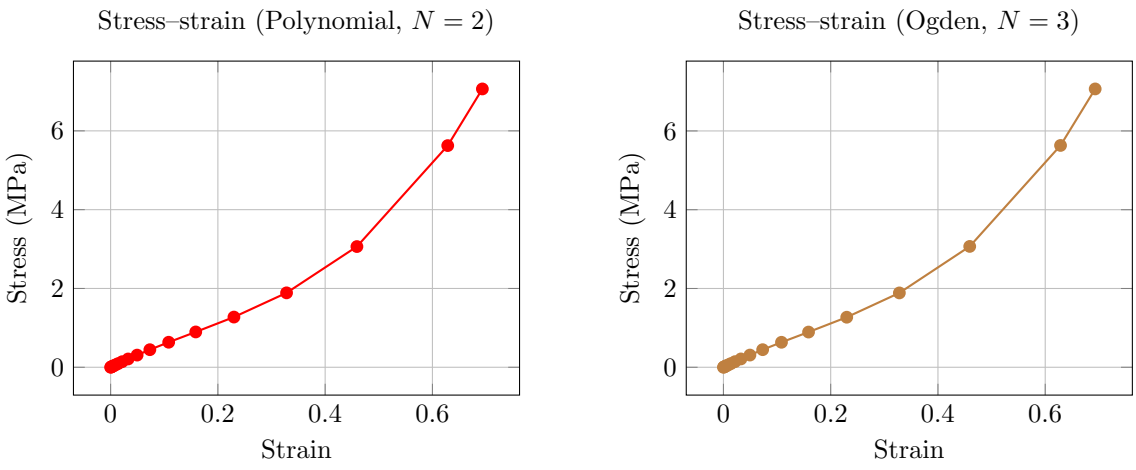

(a) Polynomial hyperelastic model ($N = 2$).

(b) Ogden hyperelastic model ($N = 3$).

Figure 7: Side-by-side comparison of stress–strain responses for two hyperelastic material models.

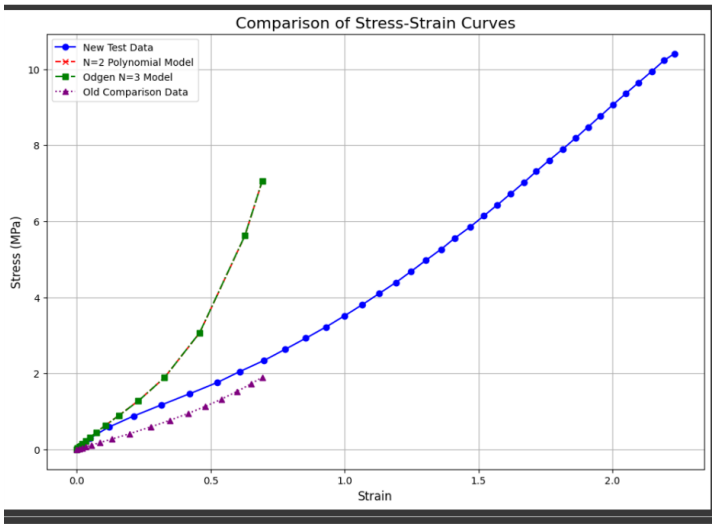

Figure 8: Comparison of Simulation results with Test data

Note that it doesn't correspond to the test data, and the stress values are very high even for small strain.

2.2 Simulating Uniaxial Tensile testing under Hydrostatic Conditions

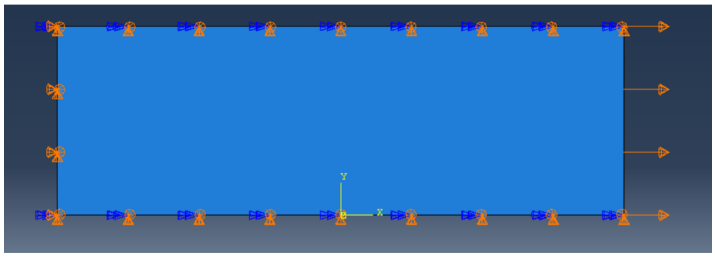

Figure 9: Model geometry and boundary conditions applied in Abaqus.

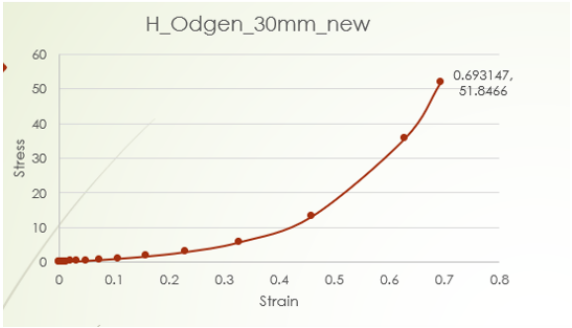

(a) H_Ogden_30mm_new

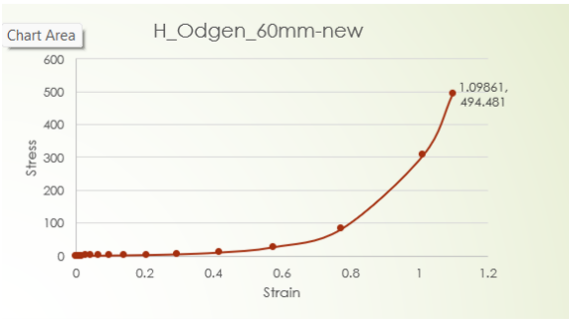

(b) H_Ogden_60mm_new

Figure 10: Stress–strain responses for Ogden models under different displacement and data conditions.

2.3 Simulating ASTM D412-06a

Test Data (same as above), changed the specimen to exactly replicate the paper results[1]

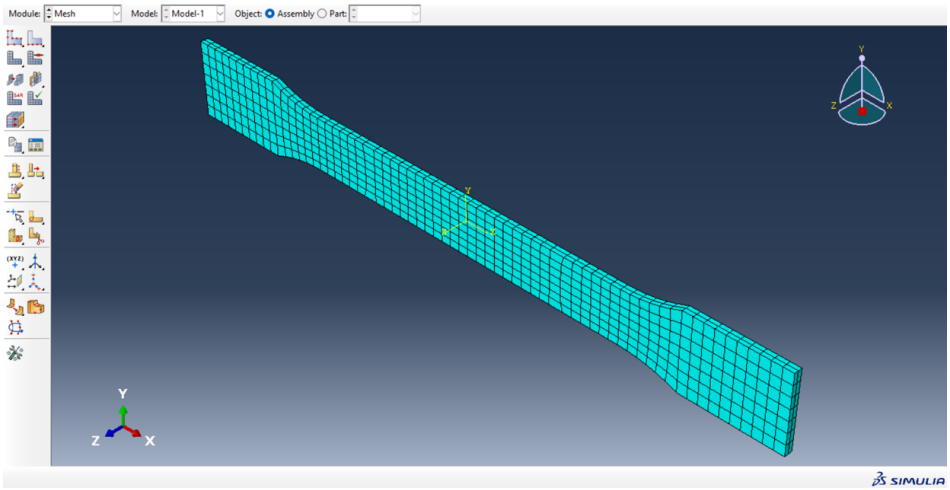

Figure 11: Mesh of the specimen: Stable for Ogden and Polynomial n=2

- For Load velocity = 0.0833mm/s (the velocity which is simulated in research paper)

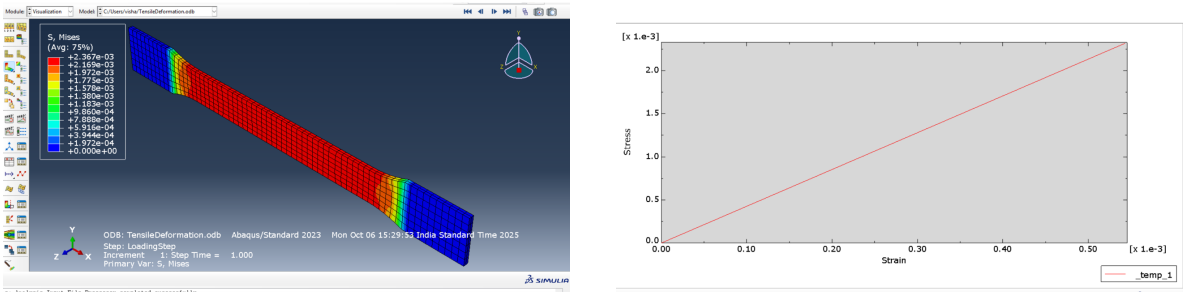

Figure 12: Simulation results for v=0.0833mm/s.(follows the paper results)

- For Load velocity = 5mm/s (the velocity which is simulated in research paper)

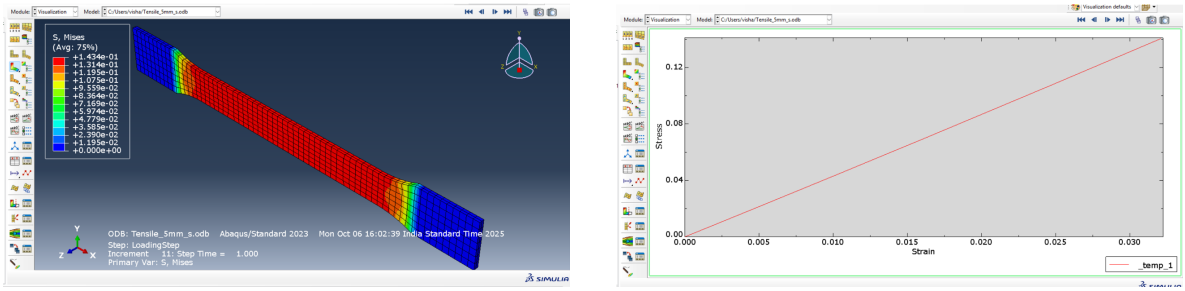

Figure 13: Simulation results for v=5mm/s (follows the paper results).

- For Load velocity = 300mm/s (the velocity which is simulated in research paper)

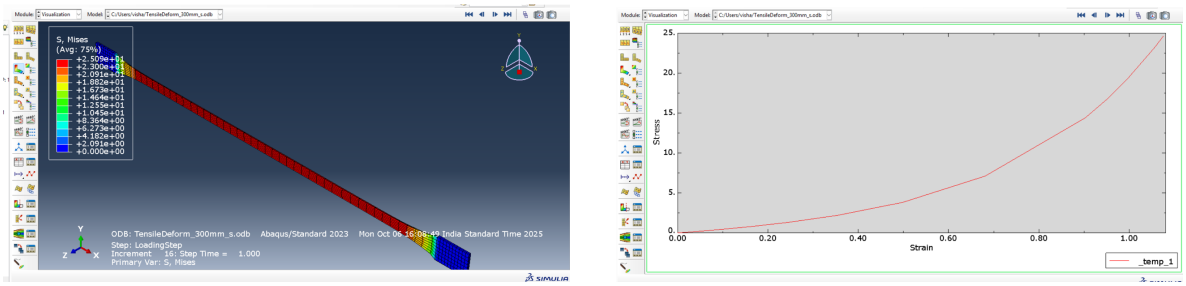

Figure 14: Simulation results for v=300mm/s (variation can be seen to start from the results in term of very high stress values).

- For Load velocity = 900mm/s: ran for 0.42% time (the velocity which is simulated in research paper)

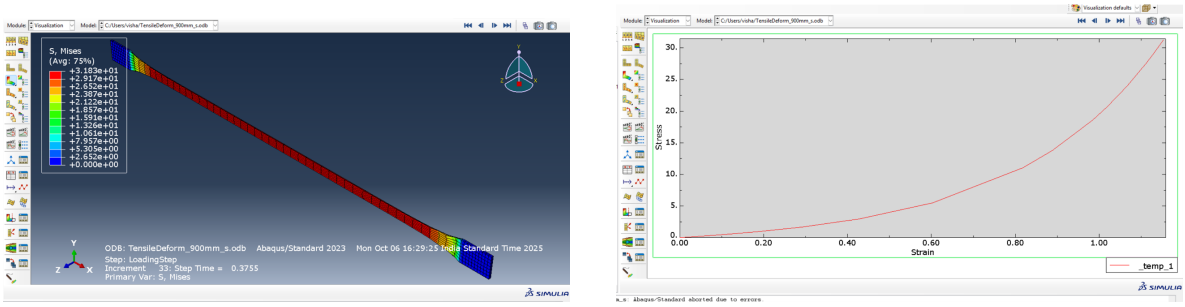

Figure 15: Simulation results for v=900mm/s (large variations can be observed).

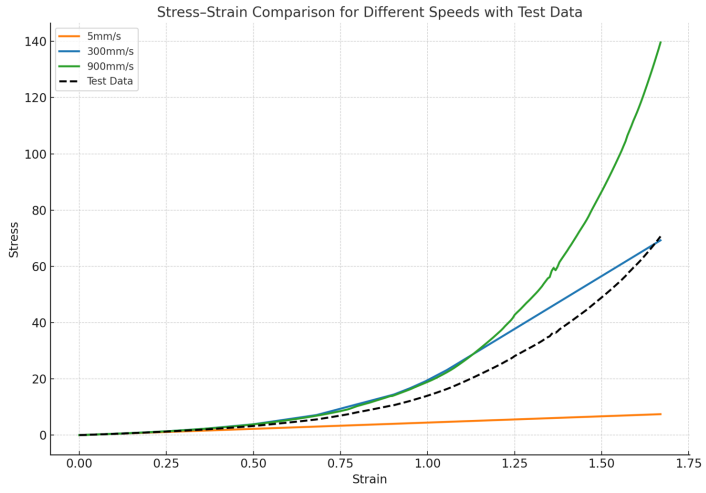

Figure 16: Comparision of Stress–strain curves for various velocities (clearly the stress values for simulation data is very high)

2.4 Simulating Uniaxial Compression for Hyperelastic Materials

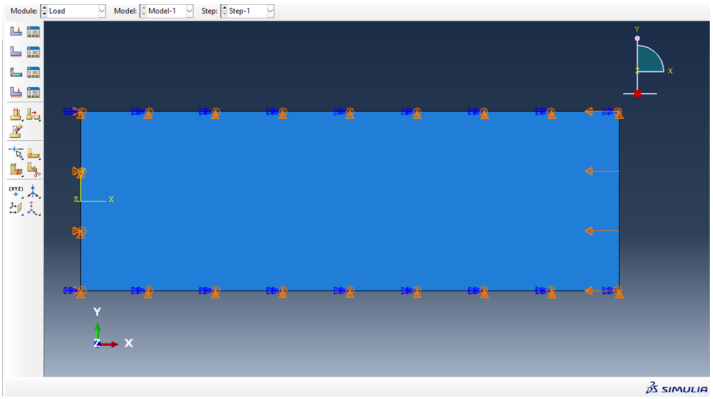

Figure 17: The boundary conditions for Compression

Couldn't find appropriate research papers for compression test data. The once found weren't stable after material evaluation.
Test Data[2]

TABLE I.—Tension in Sheet (t) and Equivalent Force of Compression for 8 % S Rubber at 20° C. Original Thickness 0·82 mm.

Air Press. P (mm.).	Radius of curvature r (cm.).	Linear Extension ratio $1/\sqrt{\alpha}$.	Compression Ratio α.	Tension in Sheet t (kg./cm. per cm.).	Equivalent Compressive force, f (kg./cm.²).
31	$3{\cdot}6_1$	$1{\cdot}02_7$*	0·95	0·92	1·02
71	$2{\cdot}5_6$	$1{\cdot}06_8$	0·88	1·50	1·93
125	2·10	$1{\cdot}11_5$	0·80	2·17	3·90
164	1·69	1·14	0·77	2·30	5·76
210	$1\ 59_8$	1 20	0·69	2·77	—
270	$1{\cdot}51_8$	1·31	0·58	3·38	10·0
304	$1{\cdot}45_4$	1·42	0·49	3·65	14·9
335	$1{\cdot}41_6$	1·68	0·35	3·93	31·3
341	$1{\cdot}42_2$	1·94	0·265	4·01	57·0
332	1·43	2·49	0·161	3·93	153
316	1·60	3·03	0·109	4·17	352
303	1·71	3·43	0·085	4·28	596
293	1·92	3·75	0·071	4·64	910
285	2·10	4·07	0·060	4·94	1360
280	2·28	4·26	0·055	5·27	1740
276	2·44	4·45	0·050	5·54	2180

* For the validity of this assumption see Holt and McPherson, *Nat. Bur. Stds. J. Res.*, 1936, **17**, 657.

This dataset provides compression derived from a validated 2-dimensional inflation method over a large strain range. The material behavior closely reflects that of nearly incompressible natural rubber, aligning with the assumptions used in the finite element model.

2.5 Simulating Uniaxial Testing for Hydroxyl-terminated polybutadiene (HTPB)

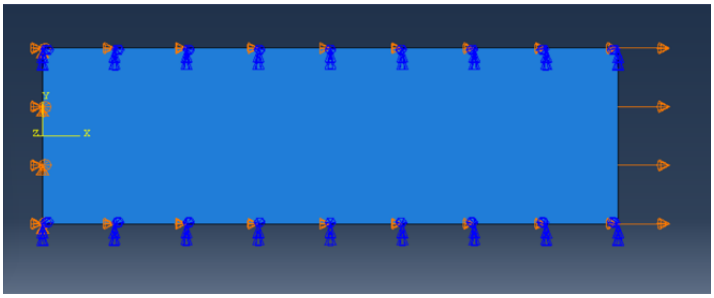

The paper[3] compares TDI- and N100-cured HTPB networks and reports their tensile modulus, strength, and elongation

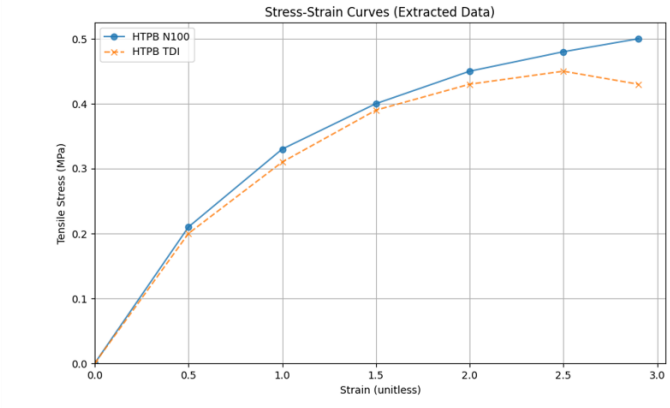

Stress–strain curves for the HTPB polymer or HTPB-based polyurethane elastomer alone, not composite propellants.
Using N100 data:

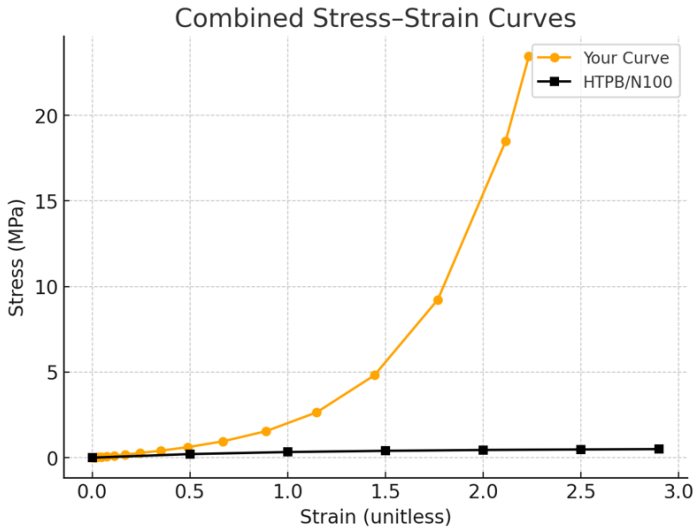

3 Conclusion

As we can see from the above comparison of simulation data with the data represented in research papers few insights come into light. Firstly, there is a great variation in the stress- strain curves of simulation and test data, posing an instant question: Ẅhy the variation? ∴ If one looks deeper, it can be seen that the simulation do obey the test pattern for small strain rate values, or small values of deformation, i.e. the linear part of the graph but as soon as these input values rise, the stress values shoot up rapidly. Thus, it can be that there is a correction term required to make test data work for simulation, or the conditions under which these analysis were performed are very specific and cannot be generalized for a simulation. In either case it raises a concern for the research work being conducted considering the test data as the preliminary stone to step on. The incorrectness can lead to heavy loss of time and delivery of faulty results. Hence, it remains an open area to research furthur on the variation seen in the simulations and the probable solutions to counteract them.

4 Literature Reviews

4.1 Constitutive modeling of the large strain time-dependent behavior of Elastomers[4]

4.1.1 Introduction

This research paper was aimed to examine carbon filled chloroprene rubber under various loading conditions and strain-rate histories. As we already know that elastomeric materials, like rubber, exhibit rate dependent mechanical behavior, i.e. they show significant hysteresis during cyclic loading and noteworthy time-dependent effects. The key issue in recurring equilibrium and time-dependent models is the inability to unable to capture the full spectrum of observed behaviors.

4.1.2 Results

- The material response becomes repeatable once the Mullins softening has been removed.
- Both filled and unfilled elastomers show significant hysteresis during cyclic loading.
- The carbon black particle content does not strongly influence the normalized amount of hysteresis (defined as the dissipated energy divided by the supplied energy during loading).
- Both filled and unfilled elastomers exhibit strong strain-rate dependence; strain-rate effects are more pronounced during uploading than unloading.
- At fixed strain, the stress tends to approach the same equilibrium stress with relaxation time, whether loading or unloading.
- The proposed model provides good quantitative predictions of the stress–strain behavior and hysteresis under uniaxial compression over a wide range of final strain levels.
- The model predicts the slow strain-rate data very well during both uploading and unloading.
- For very high strain rates, the model captures the loading response well, but the departure from equilibrium during unloading is not well predicted.
- The predicted stress relaxation rate during both uploading and unloading is in close agreement with the experimental data, and the relaxation rate is observed to decrease with relaxation time.

4.1.3 Constitutive Modeling

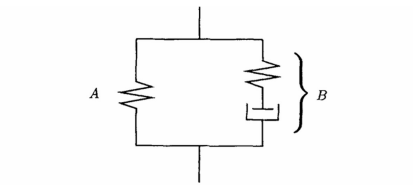

Figure 18: One dimensional rheological representation of the constitutive model

The mechanical behavior can be decomposed into two parts: an equilibrium response and a time-dependent deviation from equilibrium.
Network A is a "perfect network" and can be modeled by any of the classical models based on hyperelasticity.
Network B is here modeled as a perfect network in series with a time-dependent element that relieves the strain on the perfect network with time and captures the characteristics observed in the experimental investigation.

The total deformation gradient tensor $\mathbf{F}$ tells us how each material point moves from its reference configuration to its current configuration. Network A $\rightarrow$ represents the elastic (equilibrium) response. Network B $\rightarrow$ includes both elastic and inelastic (viscous or plastic) effects.

$$\mathbf{F} = \mathbf{F}_A = \mathbf{F}_B$$

$$\mathbf{F}_B = \mathbf{F}_B^e \mathbf{F}_B^p$$

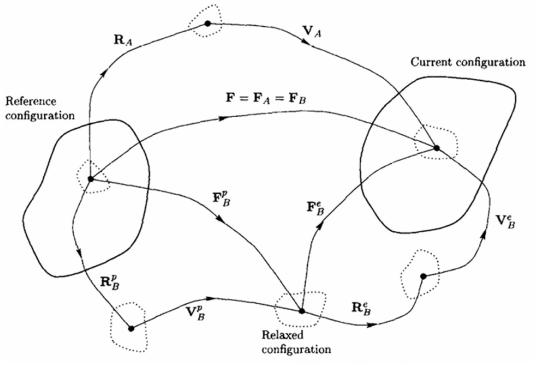

Figure 19: Multiplicative decomposition of deformation

1. Kinematics and constitutive representation of equilibrium behavior [Element (A)]

Polar decomposition for Network A:

$$\mathbf{F}_A = \mathbf{R}_A\mathbf{U}_A = \mathbf{V}_A\mathbf{R}_A$$

$\mathbf{R}_A \rightarrow$ pure rotation $\mathbf{U}_A, \mathbf{V}_A \rightarrow$ right and left stretch tensors
Here, $\mathbf{V}_A$ is symmetric, positive definite, and represents *pure stretching*.

Spectral Representation of the Stretch

The left stretch tensor for Network A, $\mathbf{V}_A$, can be expressed using its spectral representation as

$$\mathbf{V}_A = \mathbf{Q}_A \left[\sum_{i=1}^{3} \lambda_i^{(A)}\, \mathbf{e}_i \otimes \mathbf{e}_i\right] \mathbf{Q}_A^T = \sum_{i=1}^{3} \lambda_i^{(A)}\, \mathbf{I}_i^{(A)} \otimes \mathbf{I}_i^{(A)},$$

where

$\lambda_i^{(A)} \rightarrow$ principal stretches (eigenvalues), $\quad \mathbf{e}_i \rightarrow$ principal directions, $\quad \mathbf{Q}_A \rightarrow$ orthogonal rotation matrix.

Stress in Network A — Arruda–Boyce Model

For the compressible eight-chain model, the Cauchy stress component in Network A is given by

$$\sigma_i^{(A)} = C_R^{(A)}\sqrt{N^{(A)}}\,\frac{\left(\lambda_i^{(A)}\right)^2 - \left(\lambda_{\text{chain}}^{(A)}\right)^2}{\lambda_{\text{chain}}^{(A)}}\,\mathcal{L}^{-1}\left(\frac{\lambda_{\text{chain}}^{(A)}}{\sqrt{N^{(A)}}}\right) + B\ln\left(\sqrt{I_3^{(A)}}\right),$$

where

$$C_R^{(A)} = \frac{nkT}{3}, \qquad \lambda_{\text{chain}}^{(A)} = \frac{1}{\sqrt{3}}\left[(\lambda_1^{(A)})^2 + (\lambda_2^{(A)})^2 + (\lambda_3^{(A)})^2\right]^{1/2},$$

$$I_3^{(A)} = \left[\lambda_1^{(A)}\lambda_2^{(A)}\lambda_3^{(A)}\right]^2, \qquad \mathcal{L}(x) = \coth(x) - \frac{1}{x}.$$

This model contains three material parameters: the initial modulus $C_R^{(A)}$, the limiting network stretch $\sqrt{N^{(A)}}$, and the bulk modulus B.

The total stress contribution from Network A can therefore be written as

$$\mathbf{T}_A = \sum_{i=1}^{3} \sigma_i^{(A)}\, \mathbf{I}_i^{(A)} \otimes \mathbf{I}_i^{(A)}.$$

Kinematics and constitutive representation of time-dependent behavior [Element (B)]

The total velocity gradient of Network B,

$$\mathbf{L}_B = \dot{\mathbf{F}}_B \mathbf{F}_B^{-1},$$

can be decomposed into elastic and inelastic components:

$$\mathbf{L}_B = \mathbf{L}_B^e + \mathbf{F}_B^e \mathbf{L}_B^p \mathbf{F}_B^{e^{-1}} = \mathbf{L}_B^e + \tilde{\mathbf{L}}_B^p,$$

where

$$\mathbf{L}_B^p = \dot{\mathbf{F}}_B^p \left(\mathbf{F}_B^p\right)^{-1} = \mathbf{D}_B^p + \mathbf{W}_B^p, \qquad \tilde{\mathbf{L}}_B^p = \tilde{\mathbf{D}}_B^p + \tilde{\mathbf{W}}_B^p.$$

As for Network A, the left stretch tensor $\mathbf{V}_B^e$ can be decomposed as

$$\mathbf{V}_B^e = \mathbf{Q}_B^e \left[\sum_{i=1}^{3} \lambda_i^{(Be)} \mathbf{e}_i \otimes \mathbf{e}_i\right] \left(\mathbf{Q}_B^e\right)^T = \sum_{i=1}^{3} \lambda_i^{(Be)}\, \mathbf{I}_i^{(Be)} \otimes \mathbf{I}_i^{(Be)}.$$

4.1.4 Theory

Hyperelasticity

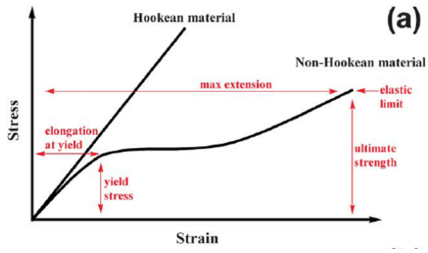

Hyperelastic materials show a non-linear stress-strain relationship, meaning their deformation isn't directly proportional to the applied force, even when they return to their original shape. Hyperelasticity is used to model materials that can undergo large, reversible deformations, such as rubbers, elastomers, and soft tissues. Hyperelastic materials use something called a strain energy density function to derive the relationship between stress and strain. This allows them to model the relationship between stress and strain accurately, even when the strain is between 100% to 700%, depending on the exact hyperelastic model that is used. Instead of defining stress directly as a function of strain, we define a strain energy density function W (energy stored per unit volume).

From W, the stress is derived mathematically as

$$\text{Stress} = \frac{\partial W}{\partial \text{Strain}}.$$

Different forms of W lead to different hyperelastic material models.
Common models include:

- **Neo–Hookean model** – simplest and often used for rubber-like materials.
- **Mooney–Rivlin model** – more accurate for large strains.
- **Ogden model** – fits a wider range of experimental data, especially for biological tissues.

Mooney–Rivlin Model

The Mooney–Rivlin model is a widely used hyperelastic material model that describes the deformation behaviour of rubber-like solids. Instead of relating stress directly to strain, the model is based on a strain energy density function W that depends on the first two invariants of the left Cauchy–Green deformation tensor. For an incompressible Mooney–Rivlin material, the strain energy density function is written as

$$W = C_1(\bar{I}_1 - 3) + C_2(\bar{I}_2 - 3),$$

where C_1 and C_2 are empirically determined material constants, and $\bar{I}_1$ and $\bar{I}_2$ are the first and second invariants of $\bar{\mathbf{B}} = (\det(\mathbf{B}))^{-1/3}\mathbf{B}$, the unimodular part of the left Cauchy–Green tensor $\mathbf{B} = \mathbf{F}\mathbf{F}^T$. The model provides a reliable representation of experimental data over a wide range of finite deformations

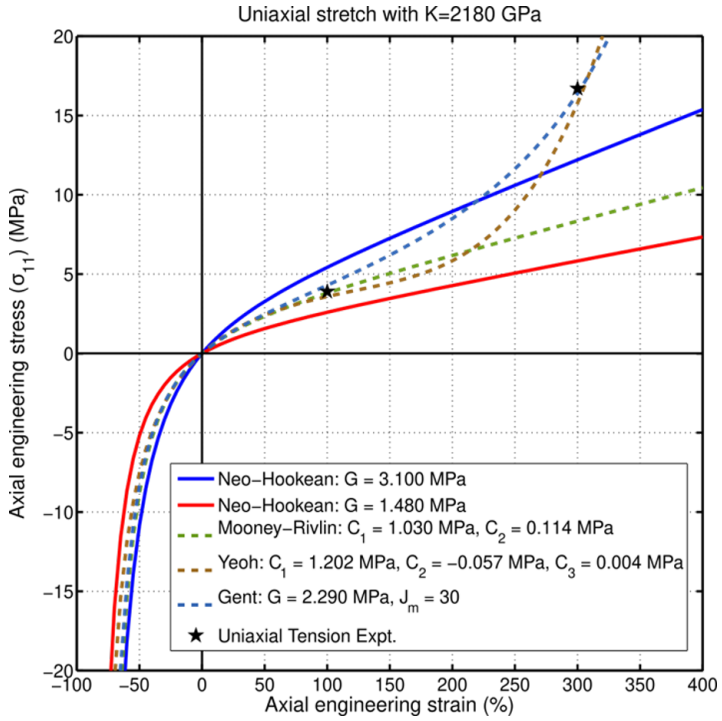

Figure 20: Stress–strain curves for various hyperelastic material models.

and is more accurate than the Neo–Hookean model for large strains. In the case of uniaxial extension, the principal stretches are $\lambda_1 = \lambda$, $\lambda_2 = \lambda_3 = 1/\sqrt{\lambda}$, and the Cauchy stress can be written as

$$\sigma_{11} = 2C_1\left(\lambda - \frac{1}{\lambda^2}\right) - 2C_2\left(\frac{1}{\lambda^2} - \frac{1}{\lambda^5}\right), \qquad \sigma_{22} = \sigma_{33} = 0.$$

For equi-biaxial tension and pure shear, similar expressions can be derived by substituting the appropriate principal stretches. These closed-form relations allow the Mooney–Rivlin model to be fit directly to experimental stress–stretch data.

4.2 The mechanical behaviour of rubber under hydrostatic compression and the effect on the results of finite element analyses[5]

4.2.1 Introduction

The models applied to hyperelastic materials are either based on a strain energy density function, for example, Mooney-Rivlin, Ogden, or Molecular-statistical approaches, for example, Arruda-Boyce, Kilian. While the usual assumptions taken: incomressible material behaviour and constant bulk modulus K (which is several orders of magnitude higher than the applied shear modulus), offers a satisfactory outcome for most of the technical applications of rubber. However when dealing with higher hydrostatic pressure values up to several 100 bar there is a large deviation between simulation results.

4.2.2 Theory

The simulation results of a unidirectional compression and tensile test for different values of the bulk modulus were compared to the results obtained by assuming incompressibility. There is no significant deviation between the resulting stresses, and hence no dependence on the bulk modulus. But when conducting the same simulation on specimens under hydrostatic pressure, the results deviate considerably.

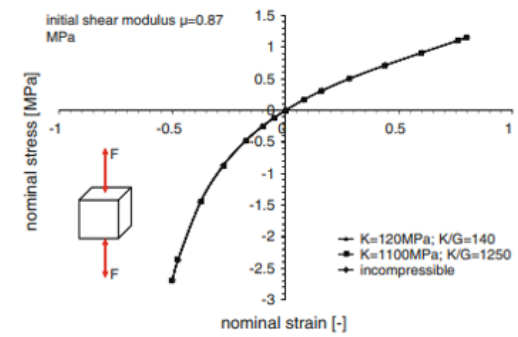

(a) Dependence of simulation result for tensile stress on bulk modulus.

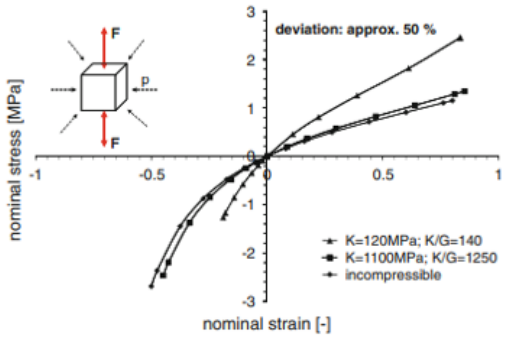

(b) Dependence of simulation result for tensile stress on bulk modulus under hydrostatic compression.

Figure 21: Comparison of simulation results for different stress responses.

Assumptions in Hyperelastic Material Modelling

Material models based on a strain energy density function commonly assume that the respective function can be split into two parts:

1. The **deviatoric, incompressible deformation** covers the isochoric change in shape due to the applied load.
2. The **volume-changing deformation** is dependent on the hydrostatic pressure.

The strain energy function is written as:

$$W = W^{\text{dev}}(\bar{I}_1, \bar{I}_2) + W^{\text{vol}}(J)$$

The Cauchy stress is expressed as:

$$\sigma = S - pI$$

The deviatoric invariants are defined as:

$$\bar{I}_1 = \bar{\lambda}_1^2 + \bar{\lambda}_2^2 + \bar{\lambda}_3^2 \qquad \bar{I}_2 = \bar{\lambda}_1^2\bar{\lambda}_2^2 + \bar{\lambda}_2^2\bar{\lambda}_3^2 + \bar{\lambda}_3^2\bar{\lambda}_1^2 \qquad \bar{\lambda}_i = J^{-1/3}\lambda_i$$

The volume ratio is:

$$J = \det(F) = \sqrt{\lambda_1^2\lambda_2^2\lambda_3^2}$$

- W^{dev}: Deviatoric (shape-changing, isochoric) part of the energy
  - Depends on invariants $\bar{I}_1$, $\bar{I}_2$ (which describe distortional changes without volume change)
- W^{vol}: Volumetric (volume-changing) part of the energy
  - Depends only on J, the determinant of the deformation gradient (a measure of volume change)
- σ: Cauchy stress tensor
- S: Deviatoric stress (from shape changes)
- p: Hydrostatic pressure (enforces incompressibility)
- I: Identity tensor

(The validity of these assumptions is examined in this paper)

4.2.3 Test bench

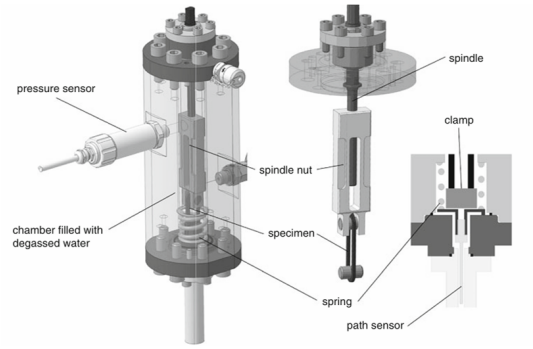

Figure 22: Test bench for conducting tensile tests under hydrostatic pressure

4.2.4 Results

- There is no influence of hydrostatic pressure up to 300 bar on the deviatoric behaviour of an NR for stretches up to 80%. Since the influence of hydrostatic pressure has proved negligible, the split of the strain energy function is valid for the investigated NR.
- The bulk modulus is an important feature to influence the outcome quality of FE simulations, especially for rubber components that are partially or completely exposed to hydrostatic pressure. For hydrostatic pressure values greater than 4 MPa, the Poisson ratio is nearly constant at 0.49992, which again clearly indicates the compressibility of the rubber component.
- The assumption of incompressibility is valid, provided that the hydrostatic pressure values are sufficiently low.

4.3 Strain hardening behaviors and mechanisms of polyurethane under various strain rate loading[6]

4.3.1 Introduction

Polyurethane is made of organic units joined by urethane bonds formed from reactions between isocyanates and alcohols. It is a chemically cross-linked copolymer with both hard and soft phases, giving it strong mechanical, physical, and chemical properties. Because of these features, polyurethane is widely used in engineering for impact-absorbing and protective structures. Experiments show it behaves like rubber at low strain rates and like glass at high strain rates, displaying strong strain-rate sensitivity. Understanding how its microstructure evolves during deformation is key to improving its mechanical performance and designing advanced polyurethane materials. Thermoplastic polyurethane (TPU), a type of polyurethane, can absorb large amounts of energy through large deformation. However, its molecular-level deformation mechanisms remain unclear due to its complex microstructure.

4.3.2 Material

Test specimens were prepared by cutting the plates using a mold designed according to the ASTM D638 Type IV standard for tensile testing.

4.3.3 Results

- Thermoplastic polyurethane (TPU) was tested under various strain rates to study its mechanical behavior. The stress–strain curves showed consistent patterns but revealed clear rate- and strain-dependent responses.
- The strain hardening ratio increased with strain rate, showing TPU becomes stronger when stretched faster.

- Numerical simulations identified the key mechanisms behind this behavior: strain-induced crystallization, chemical crosslinking, and physical entanglements. These act as hard inclusions that strengthen the material during deformation. Together, they explain TPU's strain hardening, strain dependence, and rate sensitivity, all governed by the evolving microstructure of the polymer network.
- Strain Rate Characteristics: At slow strain rates, chains have enough time to untangle and relax, leading to low hardening. At higher strain rates, chains cannot rearrange, so entanglements behave like crosslinks, increasing stiffness and hardening.
- TPU's hardening behavior depends strongly on how much it was stretched before — the larger the previous deformation, the weaker the next hardening.
- For every strain rate, n increases as strain increases, meaning TPU becomes harder as it stretches more. As the strain rate increases, n also increases — TPU hardens more quickly when it is pulled faster.

References

[1] J. Esmail, M. Mohamedmeki, and A. Ajeel, "Using the uniaxial tension test to satisfy the hyperelastic material simulation in abaqus," *IOP Conference Series: Materials Science and Engineering*, vol. 888, p. 012065, 08 2020.

[2] L. R. G. Treloar, "Stress–strain data for vulcanised rubber under various types of deformation," *Transactions of the Faraday Society*, vol. 40, pp. 59–70, 1944. [Online]. Available: https://doi.org/10.1039/tf9444000059

[3] Y. Ou, Y. Sun, and Q. Jiao, "Properties related to linear and branched network structure of hydroxyl terminated polybutadiene," *e-Polymers*, vol. 18, no. 3, pp. 267–274, 2018. [Online]. Available: https://doi.org/10.1515/epoly-2017-0223

[4] J. Bergström and M. Boyce, "Bergstroem, j.s. boyce m.c. large strain time-dependent behaviour of filled elastomers. mech. mater. 32, 627-644," *Mechanics of Materials*, vol. 32, pp. 627–644, 11 2000.

[5] J. Zimmermann and M. Stommel, "The mechanical behaviour of rubber under hydrostatic compression and the effect on the results of finite element analyses," *Archive of Applied Mechanics*, vol. 83, 02 2013.

[6] Y. Miao, H. He, and Z. Li, "Strain hardening behaviors and mechanisms of polyurethane under various strain rate loading," *Polymer Engineering Science*, vol. 60, pp. 1083–1092, 03 2020.